Available online at www.sciencedirect.com
ScienceDirect
Sensors and Actuators B 129 (2008) 79–86
SENSORS AND ACTUATORS B CHEMICAL
www.elsevier.com/locate/snb

A system for multiplexed direct electrical detection of DNA synthesis

Erik P. Anderson [a,b], Jonathan S. Daniels [a,b], Heng Yu [a], Miloslav Karhanek [a], Thomas H. Lee [b], Ronald W. Davis [a], Nader Pourmand [a,c,*]

[a] *Stanford Genome Technology Center, Stanford University, Palo Alto, CA 94304, United States*
[b] *Center for Integrated Systems, Stanford University, Stanford, CA 94305, United States*
[c] *Biomolecular Engineering, University of California Santa Cruz, Santa Cruz, CA 95064, United States*

Received 16 May 2007; received in revised form 16 July 2007; accepted 18 July 2007
Available online 2 August 2007

Abstract

An electronic system for the multiplexed detection of DNA polymerization is designed and characterized. DNA polymerization is detected by the measurement of small transient currents arising from ion diffusion during polymerization. A transimpedance amplifier is used to detect these small currents; we implemented a 24 channel recording system on a single printed circuit board. Various contributions to the input-referred current noise are analyzed and characterized, as it limits the minimum detectable current and thus the biological limit of detection. We obtained 8.5 pA RMS mean noise current (averaged over all 24 channels) over the recording bandwidth (DC to 2 kHz). With digital filtering, the input-referred current noise of the acquisition system is reduced to 2.4 pA, which is much lower than the biological noise. Electrical crosstalk between channels is measured, and a model for the crosstalk is presented. Minimizing the crosstalk is critical because it can lead to erroneous microarray data. With proper precautions, crosstalk is reduced to a negligible value (less than 1.4%). Using a micro-fabricated array of 24 gold electrodes, we demonstrated system functionality by detecting the presence of a target DNA oligonucleotide which hybridized onto its corresponding target.

Keywords: DNA biosensor; Electronic DNA microarray; DNA polymerization detection; Multiplexed current amplifier; Crosstalk

1. Introduction

Conventional DNA microarray technology utilizes lasers, optics, and fluorescent labels. These systems are bulky and ill-suited for use in a portable, rapid, point-of-care diagnostic for small-scale multiplexed detection of DNA sequences. Researchers are investigating various alternative technologies which are label-free and/or which allow miniaturization of the diagnostic device. Eliminating labels saves time and expense, particularly if PCR is not necessary to amplify the sample. Purely electronic readout is desirable because it requires relatively little space and power, can easily be multiplexed, and is low-cost. Other label-free DNA sensors detect hybridization via changes in surface impedance [4,5,14], surface charge [2,12], resonant frequency (depends on mass) [6,10,15], or index of refraction [11].

Here, we describe an electrode array and measurement electronics for the electrical detection of DNA synthesis. This can be leveraged to detect hybridization to a matched probe and/or sequence a short segment of DNA.

As described below, DNA polymerization is detected via a small transient current in a multiplexed fashion. Commercial systems are available for measuring small currents on one or two channels, but not for performing simultaneous measurements on a large array of electrodes. We characterize the sensitivity of our measuring apparatus, discuss the various noise contributions, and investigate the electronic crosstalk. We will not investigate the biological limit of detection in this paper because it depends on many factors including the surface preparation protocol, length and sequence of the probe and target strands, and duration of the hybridization.

2. Principle of detection

Direct electrical detection of DNA synthesis (or polymerization) is discussed in [13]. In summary, DNA synthesis can be detected because the incorporation of a nucleotide into the DNA

* Corresponding author at: Stanford Genome Technology Center, Stanford University, Palo Alto, CA 94304, United States.
E-mail address: pourmand@stanford.edu (N. Pourmand).

0925-4005/$ – see front matter © 2007 Elsevier Ltd. All rights reserved.
doi:10.1016/j.snb.2007.07.105

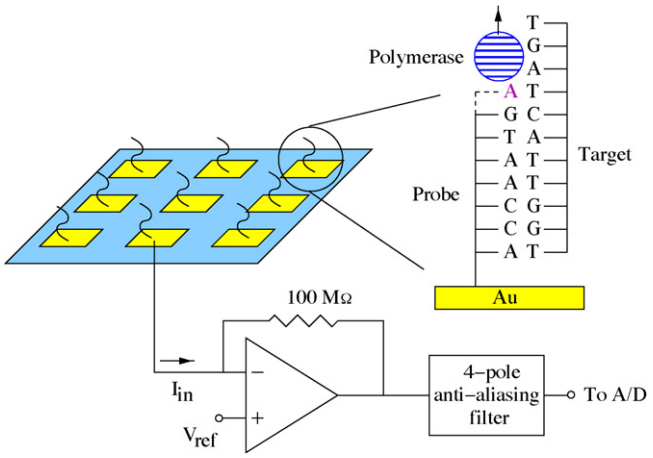

Fig. 1. The microchip array with the electronics for one channel. As the polymerase incorporates a nucleotide (an "A" here for illustration) into the DNA, a transient current is measured by the amplifier.

molecule causes a net local charge increase of 1 e^-, balanced by the generation of a proton, in proximity of an electrode. The electron is affixed to the DNA molecule and does not move. However, the proton diffuses away, causing a change in the polarization of the electrode, resulting in a transient current that may be measured by an external trans-impedance amplifier. A schematic of the system is shown in Fig. 1. Note that the measurement circuit is similar to a patch clamp circuit used for electrophysiology.

As shown in Fig. 1, an oligonucleotide (the "probe") is immobilized on an electrode. When a complementary oligonucleotide is introduced (the "target"), it hybridizes onto its corresponding probe. Polymerase enzymes are subsequently added along with the required free nucleotides needed for polymerization. For the detection method discussed in this paper, the probe and target oligonucleotide must not be the same length because we detect the incorporation of nucleotides into the double-stranded sequence during polymerization. This is not problematic because target sequences are generally longer than their corresponding probes. As an example in Fig. 1, the next base to be incorporated is an "A" as indicated by the dotted lines. When the polymerase enzyme incorporates the "A" into the DNA backbone, we measure a transient current on the electrode. Although detection of oligonucleotides in a sample is one obvious application of this technique, it may also be used to sequence a short segment of DNA with the probe serving as a primer strand and the target serving as the segment to be sequenced.

In this work, we develop a detection system composed of an array of electrodes and associated electronics, to be used in conjunction with the aforementioned detection principle. Furthermore, we demonstrate the functionality of this system by using it to detect an oligonucleotide.

3. DNA microchip

Using standard micro-fabrication techniques, a 6 by 6 grid of 300 μm square electrodes on a 600 μm pitch were deposited on a 500 μm thick quartz wafer. Twenty-four of the electrodes were gold so that thiol-modified oligonucleotides could be attached; the 12 electrodes in the center forming a "+" shape were not used in this study. Gold traces establish an electrical connection between each of the 36 electrodes and a corresponding 900 μm square contact pad located along the perimeter of the microchip, which allows each electrode to be electrically connected to an external circuit. Using a lift-off process, the gold traces are coated with silicon dioxide for insulation, while the gold electrodes and contact pads remain uncoated. Before dicing, a protective layer of photo-resist is applied, which is removed just prior to surface modification.

A custom-built socket (Synergetix, Kansas City, KS) with a clamshell-lid holds the microchip in place and provides electrical contact between the microchip and the printed circuit board electronics via doubly compressible pogo pins. The socket mounts on the underside of a printed circuit board, and a hole in the printed circuit board allows access to the electrodes. Fig. 2(b) shows the microchip sitting inside the socket without the clamshell-lid. An O-ring rests between the socket and the microchip, forming a seal and preventing liquid from leaking away from the electrodes.

3.1. Surface modification

The sensor chips were cleaned by washing with acetone and iso-propanol for 1 min each followed by a 3 min exposure to UV-ozone using a UVO cleaner (Model no. 42, Jelight Co, Irvine, CA). The sensor chips were then immersed in a 5% (w/w) (chloromethyl)phenylethyltrimethoxysilane (Gelest, Morrisville, PA) in ethanol solution with gentle shaking for 12 h. The chips were then rinsed with ethanol three times and dried in air. A 100- μM solution of probe oligonucleotides in phosphate buffer saline at pH 7.4 (0.01 M sodium phosphate, 1.0 M NaCl) was manually spotted onto the microchips and kept in a humidifier overnight, immobilizing the probes above the electrodes. The probe oligonucleotides used in this study were purchased from IDT (Coralville, IA) and have the sequence: 5′-NH_2-C_{12}-TTT TTT TTT TTG TGC CAA GTA CAT ATG ACC CTA CT-3′. After washing away unattached probes in DI water, the chips were blocked with 50 mM ethanolamine solution for 2 h at room temperature.

Target oligonucleotides at a concentration of 100 nM in a PBS buffer at pH 7.4 (sodium phosphate 0.01 M, NaCl 0.3 M) were hybridized onto the sensor chips overnight, rinsed with PBS buffer, and dried before measurements. The target oligonucleotides had the sequence: 5′-ATG CGG CAG AGC AGT GAG CTC AGC ATG TCC ATA CCA GTA GGG TCA TAT GTA CTT GGC AC- 3′.

In order to verify that the targets hybridized to their probes, a separate experiment was performed in which the targets were labeled with magnetic nanoparticles after hybridization (MACS beads, Miltenyi Biotech Inc.). An SEM image showed that hybridization indeed occurred (data not shown). Note that nanoparticle labels were necessary to verify binding because gold substrates strongly quench fluorescence [7].

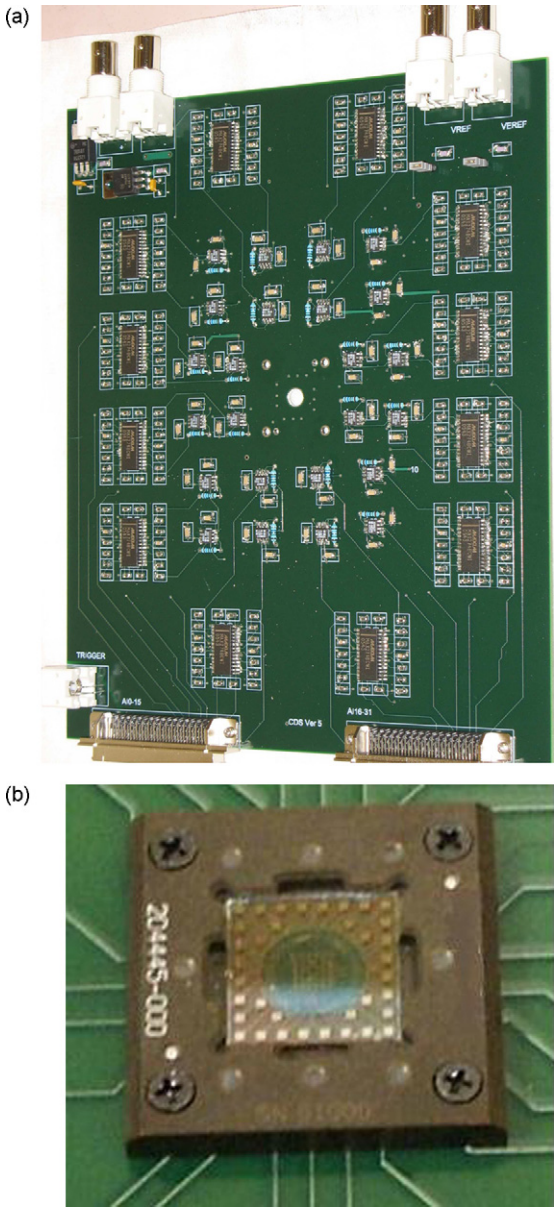

Fig. 2. Printed circuit board electronics and the socket which mounts on the underside. A hole in the center of the printed circuit board allows access to the microchip. (a) Printed circuit board electronics. (b) Microchip sitting inside the socket. Clamshell-lid is not shown. The O-ring, which provides a seal, is visible under the microchip. Note that the microchip is upside down.

4. Electronics

Fig. 2(a) shows a picture of the printed circuit board (PCB) electronics. The PCB board interfaces directly with a National Instruments 6259 16-bit data acquisition card via two SHC68-68-EPM shielded cables. The data acquisition card can acquire all 24-channels simultaneously at a maximum rate of 41.6 kHz. Furthermore, the board has a trigger output so that LabView can coordinate signal detection with dispensing of reagents onto the chip, e.g. dNTPs required for DNA polymerization.

A four-layer printed circuit board (PCB) was designed to amplify the signal from each electrode and is capable of amplifying 24 channels simultaneously. The PCB was manufactured on FR4 substrate by Advanced Circuits (Aurora, CO). Each channel consists of a transimpedance amplifier followed by a unity gain four-pole anti-aliasing filter with a −3 dB frequency of 2 kHz. Each transimpedance section uses a thick-film 100 M Ω feedback resistor for a low-frequency current-to-voltage gain of 10^8. Fig. 1 shows a schematic for one such channel.

The Analog Devices AD8627 op-amp, which has a JFET input stage, was chosen for the transimpedance stage because of its low input-referred current noise, 0.5 fA/$\sqrt{\text{Hz}}$ and voltage noise 17.5 nV/$\sqrt{\text{Hz}}$ at 1 kHz. Note that op-amp manufacturers typically specify the input-referred noise characteristics at a single frequency (typically 1 kHz). Furthermore, the AD8627 chip has a low $1/f$-noise. The input-referred noise of the op-amp ensures that the noise performance of the overall detection system will not be limited by the op-amp as discussed in Section 4.1. The Maxim MAX274, which has four 2-pole filter sections, is used to make two 4-pole anti-aliasing filters by cascading two 2-pole filters with a combined –3 dB frequency of 2 kHz. The filter also limits the noise bandwidth.

Each two-pole filter section of the MAX274 has a maximum offset voltage of ±300 mV, resulting in a maximum contribution of a four-pole filter section of ±600 mV. This dominates the maximum output offset voltage of the trans-impedance stage (given by $V_{\text{os}}^{\max} + I_{\text{b}}^{\max} R = 0.6$ mV where $V_{\text{os}}^{\max}$ =500 μV is the maximum op-amp offset voltage, $I_{\text{b}}^{\max} = 1$ pA is the maximum input bias current, and R is the 100 M Ω feedback resistor). The measured output-referred offset voltages were within ±400 mV for all channels in our system.

Fig. 3(a) shows the mean gain of the 24 amplifier channels along with gains which are three standard deviations above and below the mean. Fig. 3(b) shows the standard deviation of the amplifier gain normalized by the mean channel gain. Below 300 Hz, the normalized standard deviation of an amplifier's gain is less than 1.1%; below 4 kHz, the normalized standard deviation of an amplifier's gain is less than 4%. The design uses resistors with a 1% tolerance, and these tolerances do not fully explain the gain deviation above 300 Hz. Above 300 Hz, the main contribution to the gain deviation is chip-to-chip variations in the MAX274 filter. If required, the measured channel gains could be used to correct for the deviation in gains from channel-to-channel and thus obtain a flat frequency response, over the frequencies of interest, via post-processing of the acquired data.

Voltage regulators (7805 for +5 V, and 7905 for –5 V) from ON Semiconductor are used to regulate the Agilent E3631A power supply closer to the circuitry. The 7805 and 7905, respectively add 50 and 40 μV RMS voltage noise over 10 Hz to 100 kHz, according to the manufacturer specifications. The regulated power-supply noise was measured to be have an RMS voltage noise of 178 nV/$\sqrt{\text{Hz}}$ and a flat spectrum over the same bandwidth.

4.1. Input-referred current noise

The input-referred current noise of the electronics determines the limit of detection bound of the system (assuming the limit of detection is not set by the biology). Because, a small limit of detection is desired and because the sensor will be used to

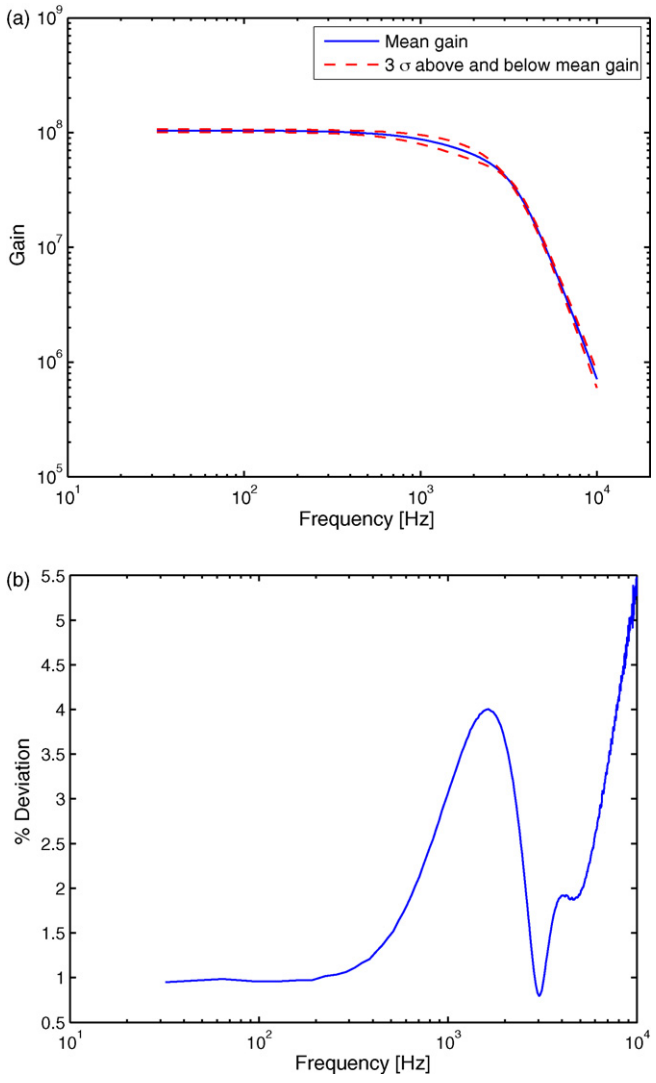

Fig. 3. Mean channel gain and the percent deviation from the mean. (a) Mean gain of all amplifier channels in V/A (b) Gain standard deviation normalized by the mean gain.

measure small currents, it is important to have as small of an input-referred current noise as possible. A good discussion of noise can be found in [8]. All noise sources in the system can be referred to the input and treated as contributions to a total input-referred current noise. Neglecting finite op-amp gain, the input-referred RMS current noise is given by calculating the output voltage noise spectral density and dividing by the transimpedance gain, R_F^2. The spectral density of the input-referred current noise is

$$\overline{I_{\text{in,tot}}^2} = \frac{4kT}{R_F} + \frac{1}{R_F^2}\left(V_f^2 + V_{oa}^2 + \frac{K_v}{f} + G_{ps+}^2 V_{ps+}^2 + G_{ps-}^2 V_{ps-}^2\right) + I_{oa}^2 \left(\frac{A^2}{Hz}\right) \quad (1)$$

where k is Boltzmann's constant, T the temperature in Kelvin, $R_F = 100\,\text{M}\,\Omega$, V_f and V_{oa} are respectively the voltage noise of the filter and op-amp referred to their respective inputs in units of V^2/Hz, I_{oa} the current noise of the op-amp referred to the op-amp input in units of A^2/Hz, and K_v is a constant which models the input-referred $1/f$ contributions to the voltage noise of the op-amp, in units of V^2. Furthermore, G_{ps+} and G_{ps-} represent the gains from the positive and negative op-amp power supply pins to the op-amp output respectively, and V_{ps+} and V_{ps-} represents the voltage noise in V^2/Hz on the positive and negative power supplies, respectively. Typically, the gains G_{ps+} and G_{ps-} are not specified on manufacturer data sheets. However, the power supply rejection ratio – the ratio between the gain from the power supply to the output and the open-loop gain – is specified on manufacturer data sheets and could be used to estimate these gains, using the data sheet value for the open loop gain of the op-amp.

For the MAX274, the specified maximum input-referred (referred to the filter input, not the channel input) RMS voltage noise for a two-pole section from 10 Hz to 10 kHz is 120 μV. Since two cascaded filter sections are used in the channel, $V_f = 2 \times 120\,\mu\text{V}/\sqrt{10\,\text{kHz}} = 2.4\,\mu\text{V}/\sqrt{\text{Hz}}$, assuming the filter noise is white. Because, $V_{oa} = 17.5\,\text{nV}/\sqrt{\text{Hz}}$ and $I_{oa} = 0.5\,\text{fA}/\sqrt{\text{Hz}}$ at 1 kHz, we expect the input-referred current noise contributions of the op-amp to be dominated by the contributions from the four-pole filter and the 100 M Ω resistor. From the AD8627 datasheet, $K_v = 3.92 \times 10^{-13} V^2$, and thus the contribution of the $1/f$-noise to the total input-referred current noise is negligible. Neglecting the noise contributions from the power supply, the maximum input-referred current noise at 300 K is

$$\begin{aligned}\overline{I_{\text{in}}^2}^{1/2} &\approx \sqrt{\frac{4kT}{R_F} + \frac{1}{R_F^2}(V_f^2 + V_{oa}^2)} \\ &= \sqrt{1.66 \times 10^{-28} + 3 \times 10^{-32} + 5.76 \times 10^{-28}} \\ &= 2.7 \times 10^{-14} \left(\frac{A}{\sqrt{Hz}}\right). \end{aligned} \quad (2)$$

Over a 2 kHz bandwidth, the total input-referred RMS current noise is 1.2 pA, excluding the power supply noise. Other potential sources of noise include $1/f$-noise in the resistor, substrate coupling, and electromagnetic interference.

The input-referred current noise for a particular channel is obtained by disconnecting the input from any sources (while the power is still applied) and measuring the output noise voltage spectral density using a spectrum analyzer. Dividing the output voltage noise spectral density (units of V^2/Hz) by the square of the channel gain (units of Ω^2) yields the input-referred current noise spectral density (units of A^2/Hz). A Stanford Research Systems SR780D spectrum analyzer was used to make the measurements. Measurements were made by averaging over 16 data sets. Note that the input-referred current noise will vary between channels because there is variation in the channel gains (Fig. 3(b)) and also in the noise contributions (e.g. the input-referred current and voltage noise will not be the same for each AD8627 op-amp).

Fig. 4 shows the measured mean input-referred current noise spectral density for all 24 channels (the system was shielded by a Faraday cage to eliminate electromagnetic interference).

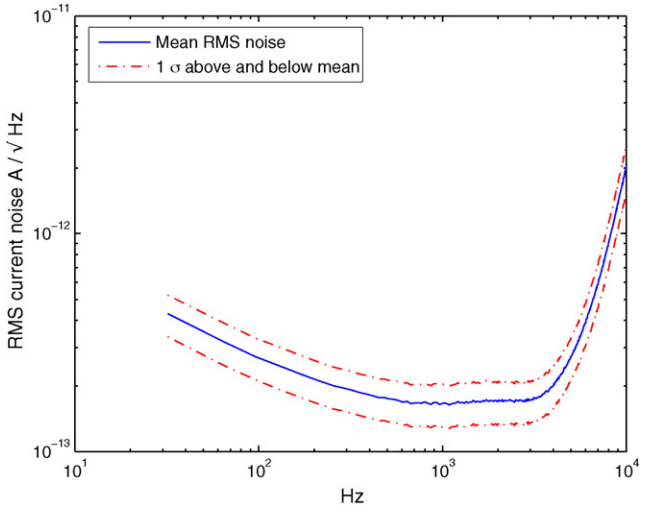

Fig. 4. The measured input-referred current noise at room temperature averaged over all 24 channels. Lowering the input-referred current noise corresponds to lowering the limit of detection. Lowering the input-referred current noise below a point will eventually limit the system performance to that set by the biological noise.

Note that the input-referred current noise is an order of magnitude worse than given by Eq. (2). Over a 2 kHz bandwidth, the measured mean input-referred current noise is 8.47 pA.

The excess noise compared to theory likely reflects noise coupled from the supply rails. The required gain from each power supply terminal to the output of the op-amp to account for the excess noise is given by

$$G_{\mathrm{ps}+,-} = \sqrt{\frac{\overline{I_{\mathrm{in,excess}}^2}}{2\overline{V_{\mathrm{ps}}^2}}}R_{\mathrm{F}} = \frac{\left(8.47\times10^{-12}(A/\sqrt{2000\,\mathrm{Hz}})\right)\times10^{8}\Omega}{2\times178\,(\mathrm{nV}/\sqrt{\mathrm{Hz}})} = 53.2 = 34.5\,\mathrm{dB} \quad (3)$$

where $\overline{V_{\mathrm{ps}}^2}$ is the noise on the power supply and the factor of 2 arises because there is both a positive and negative power supply terminal. Gains of this magnitude are not unreasonable given that open-loop op-amp gains are in excess of 120 dB (123 dB from the data sheet) and the AD8627 power supply rejection ratio is typically 104 dB with a minimum of 80 dB. Thus, the gain from *each* power supply pin to the output could be anywhere between 22 dB (i.e. 12.6) and 46 dB (i.e. 200). To test the hypothesis that the excess noise originates from that on the power supply, we measured the input-referred current noise with a power supply that had a 1000 times more noise than our Agilent E3631A supply, and as a result the input-referred current noise increased by the same order of magnitude. As a possible remedy, we replaced the Agilent power supply with 9 V batteries, but did not see any reduction in the noise; either the Agilent supply and the 9 V batteries have the same noise or the voltage regulators contribute the dominant noise to the power supply pins of the integrated circuits.

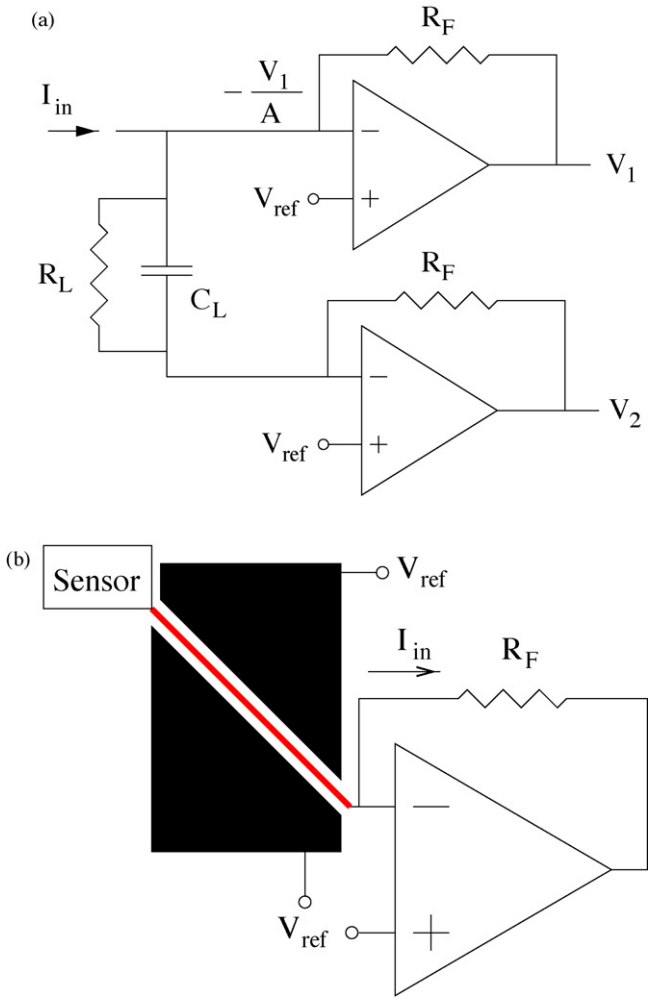

Fig. 5. A model for the crosstalk and a layout technique to reduce capacitively coupled crosstalk. (a) Crosstalk circuit model. (b) Guarding the input signal to reduce capacitive coupling. The black regions represent conducting planes surrounding the signal trace held at the same potential.

4.2. Crosstalk

In any multi-channel amplifier system, minimizing signal crosstalk between channels is an important concern. In our system, signal coupling between channels may lead one to conclude that a target DNA sequence is present at an incorrect concentration. If a current I_1 flows into the input of channel 1, then the crosstalk on channel 2 induced by channel 1 is defined as V_2/V_1, the ratio of the output voltage on channel 2 to the output voltage on channel 1. Different channels are electrically connected through the PC board and microchip substrates via the substrate resistance, R_{L}, and through the capacitance between adjacent channels, C_{L}. Fig. 5(a) shows a circuit model for the crosstalk between channels. A discussion of crosstalk in integrated circuit microarrays which sense currents is discussed in more detail in [1].

In Fig. 5(a), we assume that the input current all flows into channel 1, a good approximation if the impedance looking into channel 1, R_{F}/A, is much smaller than the impedance of the

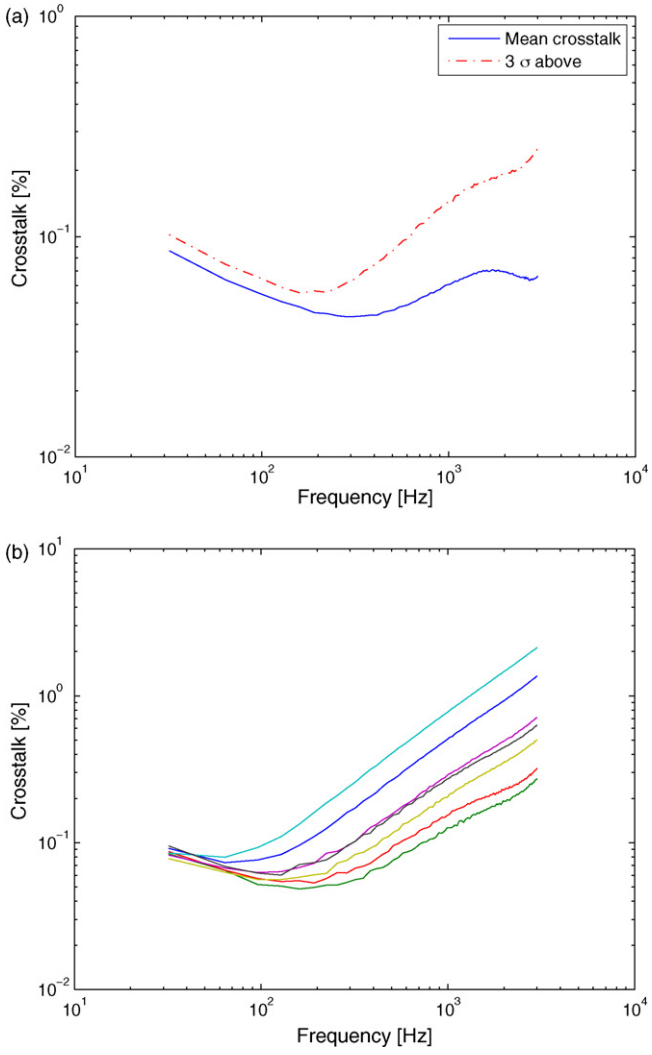

Fig. 6. (a) Crosstalk between guarded channels (sample size of 19). (b) Crosstalk between unguarded channels. Note that the crosstalk between unguarded channels follows Eq. (5).

substrate resistance and capacitance, that is if

$$\frac{R_F}{A} \ll \left| \frac{R_L}{j\omega R_L C_L + 1} \right| \tag{4}$$

where A is the finite op-amp gain and $j = \sqrt{-1}$. The crosstalk arises because the finite op-amp gain causes the potential at the inverting node of channel 1 to vary, which is then amplified by a standard inverting op-amp configuration to the output of channel 2. The op-amp holds the inverting input of channel 1 at the potential $-V_1/A$. The crosstalk voltage on channel 2 is

$$V_2 = \frac{R_F\,(j\omega R_L C_L + 1)}{R_L}\frac{V_1}{A} = -\frac{R_F^2\,(j\omega R_L C_L + 1)}{R_L}\frac{I_{in}}{A}$$
$$\approx j\omega R_F C_L \frac{V_1}{A} = -j\omega R_F^2 C_L \frac{I_{in}}{A} \tag{5}$$

where the approximation holds for frequencies that satisfy $\omega \gg 1/R_L C_L$. Fig. 6(b) shows the measured crosstalk versus frequency for several of the channels, illustrating the crosstalk follows the shape of Eq. (5) when preventative measures are not taken. Because the substrate resistance is large, the coupling impedance generally appears capacitive for frequencies as low as 60 Hz. Eq. (5) shows that crosstalk increases both with the channel gain, i.e. R_F, and frequency. The increasing crosstalk with frequency arises from a standard differentiator circuit involving the coupling capacitance C_L and the feedback resistance R_F on channel 2. Thus, there is a tradeoff between channel gain and crosstalk for a fixed substrate resistance, R_L, and capacitance, C_L. As the channel gain, R_F, increases (or equivalently as the limit of detection decreases) then the crosstalk also increases, and vice versa. In fact, for $R_F = 500\ \mathrm{M}\,\Omega$, the crosstalk between channels is 7% at 1 kHz for our system. Note that the effects of the anti-aliasing filter will have approximately the same effect on two different channels and to first-order does not affect the crosstalk. Also, note that below their unity-gain frequency, op-amps generally exhibit single-pole dynamics. For frequencies above this dominant single-pole and below the unity-gain frequency, the crosstalk will increase as ω^2 because for these frequencies the amplifier gain $A \propto 1/\omega$.

In order to reduce the capacitive coupling of Eq. (5), the PC board was designed using the guarding technique wherein the input trace is surrounded as much as possible by conductors (not physically connected to the other channel traces) held at the same potential as shown in Fig. 5(b). Due to the arrangement of the pins at the microchip socket, it was not physically possible to put a guard between every pair of adjacent traces right up to the microchip socket. Fig. 6(a) shows the mean coupling between pairs of adjacent channels from a sample of 19 measurements. Fig. 6(b) shows the capacitive crosstalk as modeled in Eq. (5) between the channels for the seven cases in which complete guarding was not possible as mentioned above. For guarded channels, the mean crosstalk from 0 to 2 kHz is less than 0.1%. For those seven cases without complete guarding, the crosstalk is still less than 1.4% over the bandwidth 0–2 kHz.

5. Signal processing

Measured signals were further processed by a digital low-pass filter to remove additional noise. We used a 236-tap Kaiser window with the parameter $\beta = 5.65$ [9], normalized to have a unity gain at $f = 0$ Hz. The null of the passband occurs at 92 Hz. Low-pass filter windows with many taps generally have shorter transition regions between the pass and stop frequency bands. The Kaiser window is used because it is maximally concentrated around $f = 0$ Hz. With the digital filtering, the input-referred current noise is reduced to 2.43 pA.

6. Measurements

Microchips were prepared according to Section 3.1 and inserted within their socket as described above, which in turn was mounted to the amplifying electronics. Note that the exposed portion of the target oligonucleotide is CC ATA CCT GTA CGA CTC GAG TGA CGA GAC GGC GTA-5′ so that the next base to be incorporated in the sequence is a G.

Forty microliter of a polymerization buffer containing 1.25 mM $MgCl_2$, 20 mM KCl, 5 mM Tris–HCl (pH 8.5) and

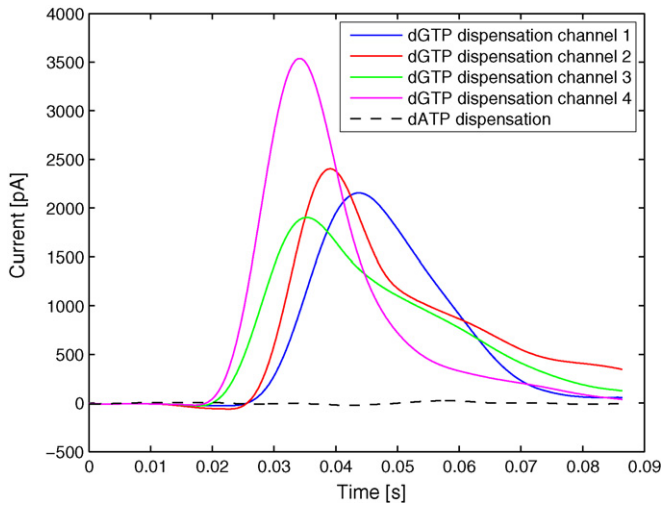

Fig. 7. The measured current after dATP and dGTP are dispensed in succession onto the microchip when the next base to be incorporated is a G. The four dGTP measurements are the signals measured on four separate electrodes which are functionalized with the probe–target pair as described in Section 3.1.

10 U Klenow exo-(Fermentas) were dispensed onto the electrodes of the microchip. The solution was allowed to equilibrate for 1 min. Next, 2 μL of dATP was placed onto the tip of a Sono-Tek ultrasonic nozzle. The ultrasonic nozzle atomized the dATPs, spraying them onto the electrode, after receiving a trigger pulse from the LabView Software. The resulting signal was recorded for each electrode at a sampling rate of 10.4 kHz.

Next, 2 μL of dGTP was placed onto the tip of the Sono-Tek ultrasonic nozzle as above and sprayed onto the microchip, and the resulting signal was recorded as the G base was incorporated into the DNA backbone. Fig. 7 shows the resulting signals when dATP and dGTP are dispensed onto the microchip in succession as discussed above. Dispensation of dATP does not result in a signal because the next base to be incorporated is a G whereas dispensation of dGTP does. Only one channel is plotted for the dATP dispensation because the other channels look similar. The resulting signal from dGTP incorporation have peaks ranging from 1903 to 3538 pA and last approximately 30–50 ms. Note that pulses which have a larger peak value also have a shorter duration. A possible explanation is a variable dGTP incorporation rate between electrodes; if the polymerases incorporate the dGTPs within a shorter timeframe, there is a larger peak current. Variation in the base incorporation rate may occur from a varying spatial distribution of polymerases above each electrode. Note that not all of the signals for dGTP dispensation start to rise simultaneously due to the variation in the time for the dGTP to diffuse to each electrode.

The control dATP measurement has a standard deviation of 21.3 pA with a peak of 51.5 pA; the standard deviation is approximately 8.8 times the mean input-referred current noise integrated over the system bandwidth. The dominant noise of the dATP control therefore is biological in origin; the noise of the electronics is much smaller than that contributed from the biology. Thus, further reduction of the electronic noise would have no system-level benefit.

7. Conclusion and further work

We developed an electrode array and associated electronics for electrical detection of DNA synthesis. We measured the input-referred current noise for each of the 24 channels of our detection system and found that the mean RMS input-referred current noise was 8.47 pA over a 2 kHz bandwidth; with digital filtering, the input-referred current noise was reduced to 2.43 pA. Although the system had higher noise than we expected, probably originating from power supply coupling, the measured biology had higher noise than the electronics; therefore, the input-referred current noise of the electronics was adequate. Furthermore, we measured the channel gains for each of the 24 channels of our system. The crosstalk between channels was typically less than 0.1% and in some cases was as high as 1.4%. We demonstrated that the system was able to measure the current resulting from DNA polymerization above an electrode.

Future work will include hybridizing a different probe strand on each electrode, using the system to detect the presence of an unknown sequence in a sample, and characterizing the biological limit of detection.

Acknowledgements

This study was supported, in part, by a grant from the National Institutes of Health, PO1-HG000205 and the National Science Foundation, DBI-0551990.

References

[1] E.P. Anderson, J.S. Daniels, N. Pourmand, T.H. Lee. Crosstalk in microarrays with current sensing, IEEE Trans. Circuit. Syst. I: Regular Papers, submitted for publication.
[2] M. Barbaro, A. Bonfiglio, L. Raffo, A. Alessandrini, P. Facci, I. Barak, A CMOS, fully integrated sensor for electronic detection of DNA hybridization, IEEE Electron Dev. Lett. 27 (7) (2006) 595–597.
[4] J.S. Daniels, N. Pourmand, Label-free impedance biosensors: opportunities and challenges, Electroanalysis 19 (12) (2007) 1239–1257.
[5] E. Katz, I. Willner, Probing biomolecular interactions at conductive and semiconductive surfaces by impedance spectroscopy: routes to impedimetric immunosensors, dna-sensors, and enzyme biosensors, Electroanalysis 15 (11) (2003) 913–947.
[6] M. Lazerges, H. Perrot, N. Zeghib, E. Antoine, C. Compere, In situ QCM DNA-biosensor probe modification, Sens. Actuat. B 120 (1) (2006) 329–337.
[7] C.Y. Lee, P. Gong, G.M. Harbers, D.W. Grainger, D.G. Castner, L.J. Gamble, Surface coverage and structure of mixed DNA/alkylthiol monolayers on gold: characterization by XPS, NEXAFS, and fluorescence intensity measurements, Anal. Chem. 78 (10) (2006) 3316–3325.
[8] T.H. Lee, The design of CMOS radio-frequency integrated circuits, 2nd ed., Cambridge University Press, Cambridge, UK, 2004.
[9] A.V. Oppenheim, R.W. Schafer, Discrete-Time Signal Processing, 1st ed., Prentice Hall, Englewood Cliffs, NJ, 1989.
[10] M. Passamano, M. Pighini, QCM DNA-sensor for GMOs detection, Sens. Actuat. B 118 (1) (2006) 177–181.
[11] K.A. Peterlinz, R.M. Georgiadis, T.M. Herne, M.J. Tarlov, Observation of hybridization and dehybridization of thiol-tethered DNA using two-color surface plasmon resonance spectroscopy, J. Am. Chem. Soc. 119 (14) (1997) 3401–3402.

[12] A. Poghossian, A. Cherstvy, S. Ingebrandt, A. Offenhausser, M.J. Schoning, Possibilities and limitations of label-free detection of DNA hybridization with field-effect-based devices., Sens. Actuat. B 111/112 (Suppl.) (2005) 470–480.
[13] N. Pourmand, M. Karhanek, H.H.J. Persson, C.D. Webb, T.H. Lee, A. Zahradnikova, R.W. Davis, Direct electrical detection of DNA synthesis, Proc. Natl. Acad. Sci. 103 (17) (2006) 6466–6470.
[14] C. Stagni, C. Guiducci, L. Benini, B. Ricco, S. Carrara, C. Paulus, M. Schienle, R. Thewes, A fully electronic label-free DNA sensor chip, IEEE Sens. J. 7 (4) (2007) 577–585.
[15] G.H. Wu, R.H. Datar, K.M. Hansen, T. Thundat, R.J. Cote, A. Majumdar, Bioassay of prostate-specific antigen (PSA) using microcantilevers, Nat. Biotechnol. 19 (9) (2001) 856–860.